Ayush Boral
Department of Aerospace Engineering,
KIIT University (KIIT-DU),
Bhubaneswar, Odisha 751024, India
e-mail: 1827014@kiit.ac.in

Souvik Dutta
Department of Aerospace Engineering,
KIIT University (KIIT-DU),
Bhubaneswar, Odisha 751024, India
e-mail: 1827065@kiit.ac.in

Anwesha Das
Department of Aerospace Engineering,
KIIT University (KIIT-DU),
Bhubaneswar, Odisha 751024, India
e-mail: 1827009@kiit.ac.in

Ankit Kumar
Department of Aeronautical Engineering,
National Formosa University,
Huwei, 632 Taiwan
e-mail: ak321531@gmail.com

Nilotpala Bej
Department of Mechanical Engineering,
KIIT University (KIIT-DU),
Bhubaneswar, Odisha 751024, India
e-mail: nilotpala2002@gmail.com

Pooja Chaubdar
Department of Aerospace Engineering,
KIIT University (KIIT-DU),
Bhubaneswar, Odisha 751024, India
e-mail: poojachaubdar94@gmail.com

Biranchi Narayana Das
Department of Aerospace Engineering,
KIIT University (KIIT-DU),
Bhubaneswar, Odisha 751024, India
e-mail: biranchi.das@kiit.ac.in

Atal Bihari Harichandan[1]
Department of Aerospace Engineering,
KIIT University (KIIT-DU),
Bhubaneswar, Odisha 751024, India
e-mail: harichandan.iitkgp@gmail.com

Drag Reduction for Flow Past Circular Cylinder Using Static Extended Trailing Edge

A numerical study has been carried out on the two-dimensional flow past a circular cylinder. In this case, a splitter plate is provided at the rear stagnation point in the downstream direction. ANSYS FLUENT *has been used to carry out the numerical simulations based on finite volume method approach. Grid independence was achieved and the numerical model was validated with results available in open literature at Reynolds numbers of 100, 5000, and 100,000 respectively. In the present investigation, the characteristics of vortex shedding due to the presence of splitter plate in the circular cylinder were investigated. The main focus of this research was to find the optimal splitter plate length for low, moderate, and high Reynolds numbers. It was observed that at low, moderate, and high Reynolds numbers, the drag coefficient (cd) for optimal plate length decreased drastically as compared to the baseline circular cylinder case. Moreover, the fluctuating nature of lift coefficient (cl) had also ceased. This research work has a good potential to decrease time-varying structural loads on bluff bodies by decreasing the vortex shedding frequency and consequently decreasing drag. The scope of our research extends to structures of bridges and large vehicles, radiator pipes of heat exchangers, landing gears of aircraft, and many more.* [DOI: 10.1115/1.4057009]

Keywords: drag, splitter plate, numerical simulation, circular cylinder, grid independence, aerodynamics, aerospace, aerospace applications, aerospace engineering, compressible flows, computational fluid dynamics, fluid flow

Introduction

The flow around basic geometries such as circular cylinders has been a topic of interest that has been extensively studied both numerically and experimentally. The phenomenon of unsteady viscous flow past a circular cylinder at different flow regimes remained challenging especially due to the complex flow physics. There are numerous real-life and engineering applications of flow past circular cylinders such as skyscrapers, bridges, landing gears of aircraft, heat exchangers, naval vehicles, periscopes, nuclear power plants, and many more. These structures experience fluid flow which induces vibrations and stresses due to the shedding of vortices. To reduce these vibrations and stresses, there is a need for a better understanding of the fluid-structure interaction. Apart from these obvious uses, it can be used in increasing accuracy of fishing gears like large-scale fishing lines and hooks as studied by Cao et al. [1]. Opinel and Srinil [2] designed a non-linear model for reporting the flow induced vibrations in a flexibly mounted circular cylinder with uniform and oscillatory inlet conditions. Petersen et al. [3] investigated numerically and experimentally to study the variation of aerodynamic loading on a circular cylinder due to secondary structures. Liu and Gao [4] studied the effect of a wall near the cylinder on the vortex shedding phenomenon.

It has been found from studies that for low Reynolds number (Re) (<47) there exist two steady recirculation zones that are symmetric to the centerline. For higher Reynolds number (>47), the recirculation zone develops and eventually sheds from the shear layer in an alternating pattern downstream of the cylinder. The process is called Von Karman vortex shedding. As the Reynolds number further increases, the transition of boundary layer from laminar to turbulent

[1]Corresponding author.

Manuscript received August 1, 2022; final manuscript received February 15, 2023; published online March 10, 2023. Assoc. Editor: Ercan Dede.

state occurs. It causes the vortices to separate further downstream of the cylinder. The delayed separation of the boundary layer results in a reduction of drag force due to the increased pressure recovery. Kang [5] observed the increase in frequency of the vortex shedding and lift fluctuations with Reynolds number. Harichandan and Roy [6] developed a novel explicit numerical scheme named Consistent Flux Reconstruction scheme using UNStructured grid for solving the incompressible N–S equation at low Reynolds number. This technique uses the information from nine neighboring cells to compute the cell center values. The pressure Poison technique was used to compute the pressure term of the momentum equations. Using the above scheme, the author studied the characteristics of three circular cylinders in a tandem and side-by-side arrangement. The behavior of lift coefficient (*cl*) and drag coefficient (*cd*) characteristics of the system of cylinders is found closely dependent on the distance separating them and their arrangements. The intriguing observation for a tandem configuration of three circular cylinders with $L = 2D$ is that the rearmost cylinder has a negative *cd* value, i.e., it experiences thrust. As the distance is increased, this phenomenon diminishes. It is noticed that the tandem cylinders have lower vortex shedding frequencies than cylinders placed side-by-side. Vortex shedding frequencies for tandem cylinders were found to be lower than cylinders placed side-by-side. Yang and Stremler [7] conducted experiments at low Reynolds number (Re) = 100 on two tandem circular cylinders in order to establish the value of the critical gap. Chen et al. [8] studied and characterized the wake pattern for two circular cylinders kept side-by-side with varying gap ratios. They identified eight distinct wake patterns for varying gap ratios. Ding et al. [9] tried the same experiment (flow past tandem and side-by-side circular cylinders) using an mesh-free least square-based finite difference (MLSFD) scheme and found that though this scheme provides robustness and flexibility, the traditional methods yield better results in some circumstances. Meneghini et al. [10] also simulated the flow past three cylinders using a fractional step method and found their results agreed with the experiments with a negative drag force in the downstream cylinders with positive drag between the gaps of two cylinders. In natural fliers like birds and insects, it has been found that their wings have a flexible trailing edge for effective flow control. These thin structures located at the trailing edge of their wing can be considered as the extended trailing edge. For example, an owl's wing has a thin extended trailing edge, which can be taken as an active flow control device that not only reduces the turbulence caused by the flapping of the wing but also reduces its noise signature. Liu et al. [11] tried using this concept on NACA 0012 wing by attaching a static extended trailing edge (SETE) behind the wing and found that it provided more lift at a smaller drag penalty than traditional flaps and gurney flaps. In the past, there have been many attempts of decreasing flow induced drag on a cylinder using passive control methodology. Imron et al. [12] found that there was a 40% decrease in drag at 5000 Re by placing an ellipse-shaped cylinder in the wake region of the cylinder. They also reported that placing a control device in the wake region is far more effective than placing it on the upstream of the cylinder. Roshko [13] used $\mathrm{Re} > 3.5 \times 10^6$ and found definite vortex shedding at Strouhal number (St) of 0.27. The separation point for a plate (or other sharp-edged shapes like wedges) is fixed at the edge, therefore variation in St and drag coefficient (*cd*) depend mainly on how Re affects the wake mechanism.

Kwon and Choi [14] used splitter plates behind a circular cylinder to control the laminar vortex shedding. With increasing plate length (l), the vortex shedding's Strouhal number gradually drops until the plate length is almost equal to the cylinder diameter (d). They noticed that the splitter plate greatly reduces net drag. They also discovered that the length of the splitter plate and the size of the primary vortex behind the cylinder are directly related to the values of the Strouhal number. Therefore, controlling the vortex shedding is very useful in practical situations. They also found that the size of the domain in the y-direction is more important than the domain size in the streamwise (x-direction) for accurately forecasting the Strouhal number. When the length of the splitter plate was greater than a critical length, the vortex shedding behind a circular cylinder vanished completely; this critical length was found to be proportional to the Reynolds number. Djebedjian et al. [15] show that the agreement between the numerical and experimental results is highly dependent on the operational conditions of the numerical solution and the obtained drag coefficients are greater than the experimental results. The authors also reported that the drag coefficients obtained by two-dimensional analysis are greater than those by three-dimensional analysis for higher values of Reynolds numbers. In this work, the unsteady laminar flow around the circular cylinder was computed using three distinct boundary conditions. The main conclusion is that the predicted drag coefficient is highly dependent on the subdivision of the boundary layer.

Liou et al. [16] implemented a splitter plate over a circular cylinder along the mid-line of wake for Re = 100,000 in their experimental and numerical works. They used an unsteady Reynolds–averaged Navier–Stokes solver with the standard high-Re turbulence model and found a non-repetitive change in the Strouhal number due to the length of the plate. The reduction of drag with the increased splitter plate length was reported to be 30% at length of plate/diameter ratio (L/D) = 1.2. They observed that as the plate length increased, the amplitude of the periodic lift force decreased significantly at high Reynolds number. Lee et al. [17] experimentally studied the effect of a small upstream control rod on the drag characteristics for a circular cylinder at Re = 20,000. They reported a 25% reduction in the total drag coefficient of the combined rod and cylinder system. On the other hand, for higher gap distances, the drag coefficient increased by 10% compared to the drag for the circular cylinder alone. Lim and Lee [18] experimentally studied the effect of O-rings on flow past circular cylinders. They experimented with different ring diameters and pitch distances and reported a maximum drag reduction of 9% at $\mathrm{Re} = 1.2 \times 10^5$. The vortices behind the O-ring cylinder show a V-shaped spanwise variation and the vortices are smaller compared to the circular cylinder case. Park et al. [19] studied the effect of small tabs attached to the upper and lower edges of the trailing edges of bluff bodies both numerically and experimentally. They reported a 33% increase in base pressure for the optimal case which eventually results in a drag reduction. Misirlioglu et al. [20] investigated the scope of passive control of the wake of a circular cylinder employing a splitter plate at Re = 500. Experimental results show that strategical position of a narrow streamwise plate behind the cylinder has potential effect to control the behavior of a bluff body wake. Moreover, the interaction between the shear layers separated from the top and bottom sides of the cylinder is suppressed due to the presence of a sufficiently long splitter plate. The generation of Karman vortices is thus prevented. Up to $L/D = 1.5$, on the bottom side of the cylinder, a vortex co-exists with a smaller vortex on the opposite side. Whereas for $L/D = 2$, the vortex of the same sign meets at the plate tip. The author's numerical results predict no drag recovery for the plate length with $L/D = 2.0$ in contrast to the experimental studies. Ozono [21] investigated the flow pattern of vortex shedding about a circular and rectangular position by placing a splitter plate asymmetrically. He studied the effects of the splitter plate placed at different longitudinal and lateral directions in the wake region. The comparison was done on the basis of Strouhal number, base suction, and peak amplitude. It was found that for some arrangements of the splitter plate, the Strouhal number surpassed the natural value. It was also found that the asymmetrical placement of the plate behind the cylinder reduced the occurrence of the vortex phenomenon. The increase in Strouhal number is explained by the separation of the shear layer. Vu et al. [22] simulated flow past a circular cylinder with splitter plate. They reported that the vortex shedding disappears when the length of the splitter plate is greater than a critical value and this value is dependent on the Reynolds number of the flow. They found that the *cd* decreases more significantly at higher Re. Barman and Bhattacharyya [23] studied the effect of dual splitter plates attached to a square cylinder. They reported that the upstream

plate can lead to significant drag reductions and the downstream plate dampens the vortex shedding frequency. They found that at $\mathrm{Re} = 150$, the placement of upstream and downstream splitter plates can both reduce drag as well as vortex shedding frequency. Pang et al. [24] tested different turbulence models in ANSYS FLUENT to get the optimal model for high Reynolds number in the order of 5.2×10^6 around a 2D cylinder. They found that the k–ω SST model gives the best results for Strouhal number and angle of vortex shedding. They further tested with curvature correction on this model. The numerical results agreed further with the experimental findings. Amalia et al. [25] identified the best turbulence model by analyzing the flow in a circular cylinder and the impact of time-step size on the flow. According to their findings, the optimal outcome can be achieved with the SST k–ω turbulence model for 2D case and time-step between 0.00025 s and 0.004 s is preferred. For the 3D case, Reynolds stress was found to be the superior scheme giving results closer to the experimental value. Time-step between 0.00025 s and 0.0005 s is preferred with smaller time-step yielding better results. Based on the findings of these literature, the SST k–ω turbulence model was selected for the current study.

It has been noticed from the existing open literature that not much research work has been conducted on the effect of trailing edge on flow past a circular cylinder at low and moderate Reynolds numbers. Thus, the influence of an SETE on a circular cylinder has been investigated numerically at different Reynolds values in this article. This research is aimed to find the optimal plate length to inhibit the time-varying nature of lift and drag caused due to the shedding of vortices. Upon verifying the results due to a circular cylinder having zero plate length (L) to diameter (D) ratio, the simulation was carried out for Reynolds numbers 100, 5000, and 100,000. Then, the plate length was increased from $L/D = 0$ to 2 with an increment of $L/D = 0.1$.

This research can be further extended to complex aero-acoustics problems where noise and vibrations generated due to vortex shedding are a major drawback. Duan and Wang [26] studied the control of flow induced noise using a rigid and flexible splitter plate for a circular cylinder. They reported that for Re of the order of 10^4–10^5, $L/D = 1.0$ is the optimal plate length for noise reduction. Another scope of this research is to study the effect of extended trailing edge on the heat transfer characteristics for a heated circular cylinder. For flow past circular cylinder, vortex shedding promotes enhanced mixing and momentum transfer and causes increased heat transfer. However, if the vortex shedding is suppressed, then it is expected that the heat transfer will reduce. This analysis can be done by imposing a constant temperature Dirichlet boundary condition on the walls. Such an analysis will be more computationally expensive since the energy equation will also come into the picture. The flow behavior inside a duct with a cavity and moving walls with convective heat transfer were studied numerically by Mebarek-Oudina et al. [27]. Similar numerical formulation can be used to simulate the flow past a heated circular cylinder with a trailing edge. The computational results can be compared with the similarity solution analysis of thermal boundary layer using the Taylor series expansion model formation, Djebali et al. [28], and it can be analyzed if the wake flow near the trailing edge admits similarity solution. Asogwa et al. [29] examined the influence of volume fractions of different water-based nano-fluids on the heat transfer characteristic for flow over a Riga plate. Nano-fluid flow past a radiative circular cylinder was studied by EL-Zahar et al. [30].

Governing Equations

The turbulent kinetic energy and specific dissipation rate are calculated using the SST k–ω turbulence model as proposed by Menter [31] as follows:

Turbulent kinetic energy

$$\frac{\partial \rho k}{\partial t} + \frac{\partial \rho u_j k}{\partial x_j} = P - \beta^* \rho \omega k + \frac{\partial}{\partial x_j}\left[(\mu + \sigma_k \mu_t)\frac{\partial k}{\partial x_j}\right]$$

Specific dissipation rate

$$\frac{\partial \rho \omega}{\partial t} + \frac{\partial \rho u_j \omega}{\partial x_j} = \frac{\gamma}{\nu_t} P - \beta \rho \omega^2 + \frac{\partial}{\partial x_j}\left[(\mu + \sigma_\omega \mu_t)\frac{\partial \omega}{\partial x_j}\right] + 2(1 - F_1)\sigma_{\omega 2}\frac{\rho}{\omega}\frac{\partial k}{\partial x_j}\frac{\partial \omega}{\partial x_j}$$

$$P = \tau_{ij}\frac{\partial u_i}{\partial x_j}$$

$$\tau_{ij} = \mu_t\left(2S_{ij} - \frac{2}{3}\frac{\partial u_k}{\partial x_k}\delta_{ij}\right) - \frac{2}{3}\rho k \delta_{ij}$$

where τ_{ij} is Reynolds stress tensor.

$$S_{ij} = \frac{1}{2}\left(\frac{\partial u_i}{\partial x_j} + \frac{\partial u_j}{\partial x_i}\right)$$

Turbulent eddy viscosity (ν_t) is computed from

$$\nu_t = \frac{\rho a_1 k}{\max(a_1 \omega,\ \Omega F_2)}$$

Each of the constants is a blend of inner (1) and outer (2) constant

$$\Phi = F_1 \Phi_1 + (1 - F_1)\Phi_2$$

where Φ_1 represents constant 1 and Φ_2 represents constant 2

F_1 (blending function)

$$F_1 = \tanh\left\{\left\{\min\left[\max\left(\frac{\sqrt{k}}{\beta^* \omega y}, \frac{500\nu}{y^2 \omega}\right), \frac{4\rho\sigma_{\omega 2} k}{CD_{k\omega} y^2}\right]\right\}^4\right\}$$

$$\mathrm{CD}_{k\omega} = \max\left(2\rho\sigma_{\omega 2}\frac{1}{\omega}\frac{\partial k}{\partial x_j}\frac{\partial \omega}{\partial x_j}, 10^{-20}\right)$$

F_2 (second blending function)

$$F_2 = \tanh\left[\left[\frac{2\sqrt{k}}{\beta^* \omega y}, \frac{500\nu}{y^2 \omega}\right]^2\right]$$

where y is the distance from the field point to the nearest wall.

In the current simulations,

$$\rho \text{ (density of air)} = 1.225 \text{ kg/m}^3$$

$$\mu \text{ (dynamic viscosity of air)} = 1.7894 \times 10^{-5} \text{ kg/m} \cdot \text{s}$$

$$\nu \text{ (kinematic viscosity of air)} = 1.4607 \times 10^{-5} \text{ m}^2/\text{s}$$

$$a_1 \text{(constant)} = 0.31$$

For near wall region

$$\sigma_{k1} = 0.85,\ \sigma_{\omega 1} = 0.65,\ \beta_1 = 0.0750,\ \beta^* = 0.09,\ k = 0.41,$$

$$\gamma_1 = \beta_1/\beta^* - \sigma_{\omega 1} k^2/\sqrt{\beta^*}$$

For free shear layers

$$\sigma_{k2} = 1.0,\ \sigma_{\omega 2} = 0.856,\ \beta_2 = 0.0828,\ \beta^* = 0.09,\ k = 0.41,$$

$$\gamma_2 = \beta_2/\beta^* - \sigma_{\omega 2} k^2/\sqrt{\beta^*}$$

For general flows, Ω is taken to be the absolute value of vorticity.

Geometrical Description of the Computational Flow Domain

In the current study, a rectangular domain was selected. The diameter (D) of the cylinder was taken as 0.1 m. The inlet, and the top and bottom surfaces were at a distance of 8D from the center of the cylinder. The outlet was located 25D away from the cylinder's center (Fig. 1).

Problem Definition, Numerical Model, and Initial Boundary Conditions

The unsteady incompressible Navier–Stokes equation for two-dimensional flow was solved by SIMPLE discretization scheme and second-order implicit transient formulation. In the current research, SST k–ω turbulence model was employed. Unstructured grid was used to establish the basic numerical model and to validate the same for the present problem.

The values of velocity and pressure are specified as the boundary conditions at the inlet and outlet of the geometry respectively. No-slip boundary condition is specified at the surface of the cylinder whereas the upper and lower boundaries are specified as moving walls. The velocity of the moving wall is considered to be the same as the freestream velocity. The authors first considered structured mesh for the simulation as it provided an appropriate spatial; discretization needed for accurate results but the skewness of the mesh would increase significantly when a splitter plate would be introduced. Thus, the unstructured mesh was considered for the current study (Fig. 2).

Grid Independence Study

The grid independence of the computational domain is verified on the unstructured mesh using SST k–ω turbulence model at Re = 5000 for validating our numerical model for finding the optimum mesh for numerical simulation. Coefficients of lift, drag, and Strouhal numbers have been reported and compared.

Table 1 shows the results for the SST k–ω turbulence model for unstructured grid for choosing the most optimum grid based upon the percentage change in coefficient of drag. The percentage change was computed with respect to the mesh with highest number of cells. The variation of Y component of velocity measured in the near-wake region ($x = 0.2$ m, $y = 0.05$ m measured from the center of the cylinder) is shown in Fig. 3. The authors selected the second grid having 180,296 elements for further cases using the SST k–ω turbulence model. The grid chosen to run the simulation has to be validated with existing literature at varying Reynolds numbers. After conducting the grid independence study for 5000 Reynolds number, the model was validated for both 100 and 100,000 Reynolds numbers.

Table 1 Grid independence test for SST k–ω turbulence model using unstructured grid

	Number of cells	*cl*	*cd*	St	Percentage change in *cd*
1	48,792	−0.03	1.31	0.21	3.5
2	180,296	0.01	1.37	0.21	0.63
3	271,269	−0.00	1.35	0.21	0.43
4	471,778	0.01	1.36	0.21	0

Table 2 shows the flow parameters, i.e., coefficients of lift, drag, and Strouhal number for flow past single cylinder at Re = 100 is reported and compared with existing literature. At Reynolds numbers 5000 and 100,000, the coefficient of drag and Strouhal number are reported to verify the grid being considered. The present result is compared with existing results, and the values are found to be in good agreement. After the validation, further numerical simulation for varying plate lengths is done to determine the optimum plate length (Tables 3 and 4).

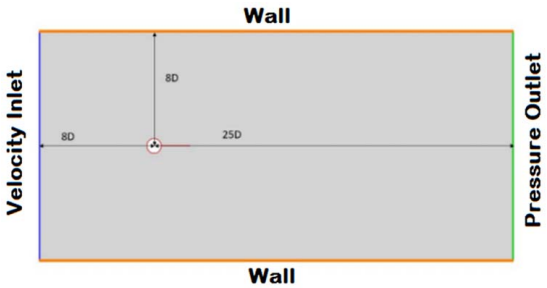

Fig. 1 Geometry of the flow domain

Results and Discussion

In the current study, the flow around a single circular cylinder with a splitter plate, termed as SETE, attached to the rear surface is simulated using ANSYS FLUENT 2019 R3 for varying lengths of the plates at three different values of Reynolds numbers. The Reynolds numbers considered for the current analysis are 100 (low Reynolds number flow), 5000 (moderate Reynolds number flow), and 100,000 (high Reynolds number flow). Flow parameters like lift and drag coefficients and the Strouhal numbers have been reported and the change in lift and drag coefficients have been reported and analyzed. Vorticity contours have been analyzed to observe and analyze the Karman vortex street.

In the current study, optimal plate length is defined as the minimum possible plate length at which the vortex shedding phenomenon drastically reduces or stops. Because of reduction in vortex shedding, the *St*, *cl* (RMS), and *cd* (avg) all decrease. The minimum possible plate length which satisfies these parameters is considered the optimal plate length.

Cylinder Attached With SETE Attached at Reynolds Number 100. The flow past cylinder at low Reynolds number has a lot of unique and attractive features but adding a splitter plate adds a whole new level of complexity in flow field in the wake of the cylinder. Twenty different lengths of plates have been added and analyzed to study the flow features. The change

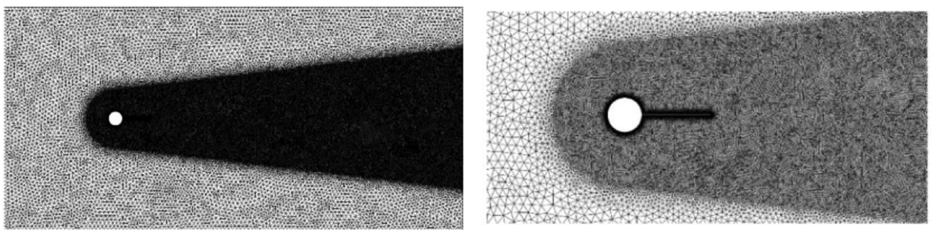

Fig. 2 Computational model and close-up view of the circular cylinder

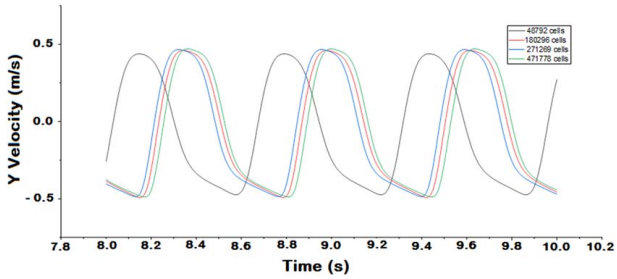

Fig. 3 *Y* component of velocity for different mesh fineness

Table 2 Values of flow parameters for flow past single circular cylinder at Re = 100

	Coefficient of drag	Coefficient of lift	Strouhal number
Harichandan and Roy [6]	1.352 ± 0.010	±0.278	0.161
Kang [5]	1.33 (RMS)	0.228 (RMS)	0.165
Ding et al. [9]	1.356 ± 0.010	0.287 (RMS)	0.166
Meneghini et al. [10]	1.370 ± 0.010	—	0.165
Braza et al. [32]	1.364 ± 0.015	±0.25	0.16
Tritton [33]	1.320 ± 0.010	—	0.16
Wiesenberger [34]	1.326 ± 0.010	—	0.1608
Present result	1.349 ± 0.004	±0.21	0.16

Table 3 Values of flow parameters for flow past single circular cylinder at Re = 5000

	Coefficient of drag	Coefficient of lift	Strouhal number
Ahlborn et al. [35]	—	—	0.21
Imron et al. [12]	1.51	—	—
Widodo et al. [36]	1.51	—	—
Aljure et al. [37]	1.12	—	0.21
Present result	1.37 ± 0.1	±1.28	0.21

Table 4 Values of flow parameters for flow past single circular cylinder at Re = 100,000

	Coefficient of drag	Coefficient of lift (RMS)	Strouhal number
Cox et al. [38]	—	—	0.24
Zan and Matsuda [39]	0.624	0.173	0.251
Present result	0.7 ± 0.01	0.23	0.24

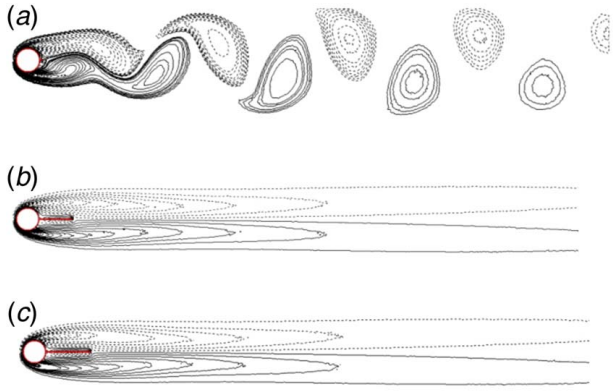

Fig. 5 Vorticity contours of flow past circular cylinder at Re = 100: (*a*) plate length (*L*/*D*) = 0.1, (*b*) plate length (*L*/*D*) = 1.5, and (*c*) plate length (*L*/*D*) = 2.0

in coefficients of lift and drag, and the Strouhal number have been reported and are compared with results of the flow parameters of a single isolated cylinder without any splitter plate at the rear surface.

First, the authors simulated a single isolated cylinder at Reynolds number 100 and reported the flow parameters in which the maximum coefficient of lift achieved is 0.21 and the minimum coefficient of lift achieved is −0.21. When the single cylinder is attached with SETE and simulated numerically by varying lengths of splitter plate, the flow parameters are different, and the flow contours vary depending upon length of the plate. Twenty different lengths of plates have been considered and are simulated for Reynolds number 100. The results show that the maximum coefficient of lift (RMS) achieved when the length of plate (*L*/*D*) is 0.2 and 0.3. The coefficient of lift then starts decreasing with increasing plate's length and becomes zero when the length of plate (*L*/*D*) exceeds 1.3 as observed from Fig. 4. On the contrary, the drag coefficient shows a uniform decreasing behavior with increasing the plate's length as shown in Fig. 4. The Strouhal number starts decreasing when the length of plate (*L*/*D*) exceeds 0.2. Figure 5 shows the vorticity contours for the cylinder attached with SETE for varying plate lengths. The vortex shedding phenomenon in the downstream of the cylinder is delayed due to the splitter plate and the delay increases with increasing the length of SETE.

At *L*/*D* = 0.1 for Reynolds number 100, a Karman vortex sheet can easily be observed in the downstream of the cylinder due to the vortex shedding. In the same case, a reduction and an increase in coefficients of drag and lift of about 0.26% and 7.53% have been observed respectively and the Strouhal number remains almost constant. When the *L*/*D* is increased to 1.5, the vortex shedding stops abruptly and two huge vortices are generated which extend to the downstream of cylinder as observed from Fig. 5. A decrease of 12.51% in coefficient of drag, 99.10% decrease in coefficient of lift, and a decrease of 62.89% in Strouhal number has been observed for *L*/*D* = 1.5 case. This case is the optimal plate length

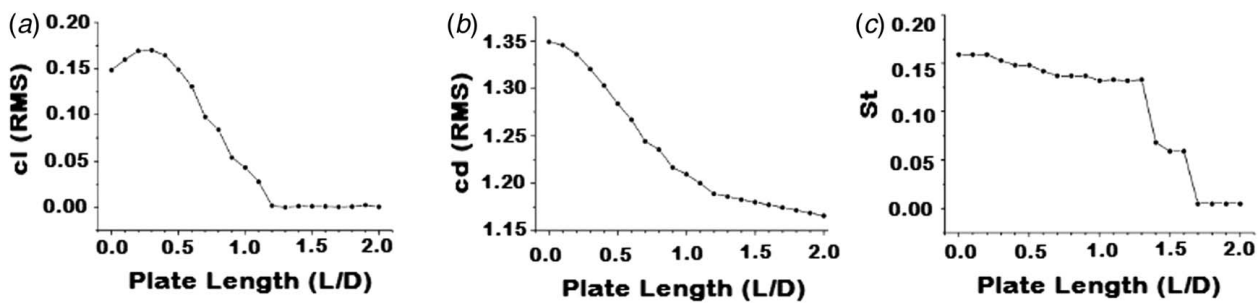

Fig. 4 (*a*) Coefficient of lift, (*b*) coefficient of drag, and (*c*) Strouhal number for a cylinder attached with SETE at Re = 100

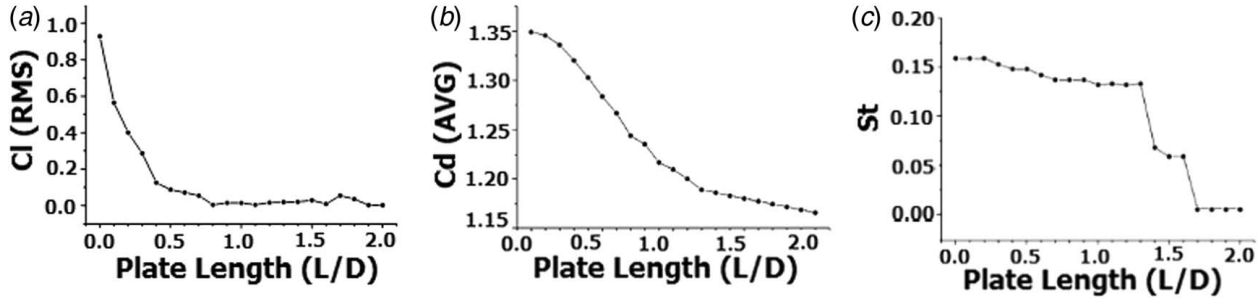

Fig. 6 (*a*) Coefficient of lift, (*b*) coefficient of drag, and (c) Strouhal number for cylinder attached with SETE at Re = 5000

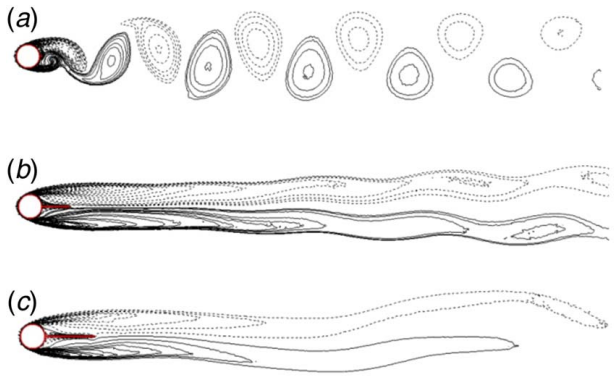

Fig. 7 Vorticity contours of flow past circular cylinder at Re = 5000: (*a*) plate length (*L/D*) = 0.1, (*b*) plate length (*L/D*) = 1.2, and (*c*) plate length (*L/D*) = 2.0

since *cl* (RMS) and *cd* (avg) and St are considerably low and the vortex shedding has stopped as observed from Fig. 5.

Cylinder Attached With SETE Attached at Reynolds Number 5000. Flow past a cylinder for Reynolds number 5000 has been simulated and the flow contours and parameters have been analyzed for understanding the nature of flow for varying plate lengths. Twenty different lengths of plates have been added and analyzed for studying the flow field. In the current case, the results have been reported and compared with the flow past an isolated cylinder without attaching SETE as in the previous case.

The highest lift coefficient achieved is ±1.28 for the flow past an unconfined cylinder. Then it lowers drastically when splitter plate is attached to the cylinder. The lowest coefficient of lift is achieved when the plate length (*L/D*) is 1.4 and then starts increasing at a slow rate. The coefficients of lift and drag are decreasing with increasing length of plate as observed from Fig. 6. The Strouhal number constantly decreases with increase in the plate's length and reaches its minimum at plate length (*L/D*) of 2.0. Figure 7 shows vorticity contours for isolated cylinders attached with SETE of varying length at Reynolds number 5000. The contours show the vortex shedding and generation of Von Karman vortex Street. The vortex shedding starts to delay as the length of the SETE increases.

At L/D = 0.1 for Reynolds number 5000, a vortex sheet is observed in the downstream of the cylinder and a decrease of 17.35% in coefficient of drag, decrease of 39.28% in coefficient of lift, and a decrease of 0.95% in Strouhal number has been observed. When the *L/D* increases to 1.2, the vortex shedding stops and two huge vortices are generated in the downstream of the cylinder which extends toward downstream. Fluctuations are observed in the downstream and the results show a decrease of 40.195% in coefficient of lift, decrease of 98.24% in coefficient of drag, and a decrease of 55.71% in Strouhal number for plate length (*L/D*) of 1.2. For this case, two stable attached vortices are found on the downstream of the cylinder. From Fig. 6, it can be observed that for this case the *cl* (RMS), *cd* (avg), and St are considerably low. Moreover, from the vorticity contours in Fig. 7, it can be observed that the vortex shedding phenomenon has stopped. So, *L/D* = 1.2 is the optimal plate length case. Strouhal number further decreases with an increase in the length of the plate.

Cylinder Attached With SETE Attached at Reynolds Number 100,000. Flow past an isolated cylinder at Reynolds number 100,000 has been simulated and the flow contours and parameters have been analyzed for understanding the complexities of the resultant flow. The flow past circular cylinders is attached with SETE of varying plate lengths. Twenty different lengths of plates have been added and analyzed to study the flow field downstream of the cylinder. For the current case, the results have been reported and then compared with flow past an isolated cylinder without attaching SETE as in previous two cases.

The lift coefficient then decreases drastically with increasing the length of the plate. The coefficients of lift and drag are not uniform and show a fluctuating nature. Both lift and drag coefficients attain a minimum at *L/D* = 0.6. On the contrary, the Strouhal number decreases gradually with increasing the length of plate. After *L/D* = 0.5, the Strouhal number drastically decreases. Figure 9

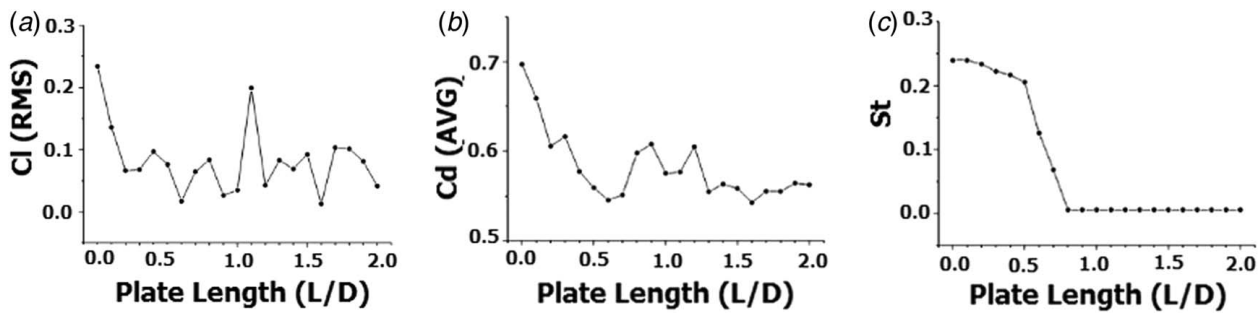

Fig. 8 (*a*) Coefficient of lift, (*b*) coefficient of drag, and (c) Strouhal number for cylinder attached with SETE at Re = 100,000

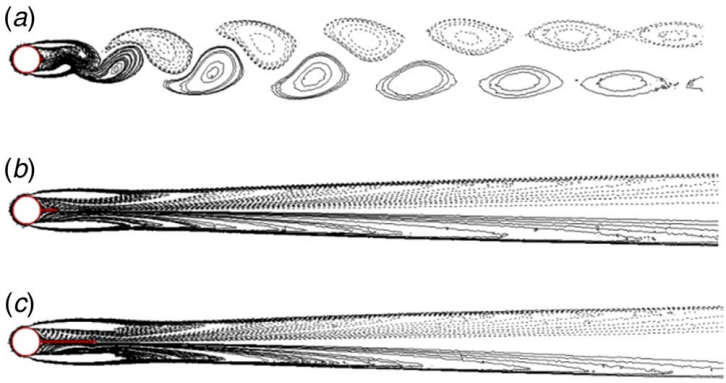

Fig. 9 Vorticity contours of flow past circular cylinder at Re = 100,000: (*a*) plate length (*L*/*D*) = 0.1, (*b*) plate length (*L*/*D*) = 0.6, and (c) plate length (*L*/*D*) = 2.0

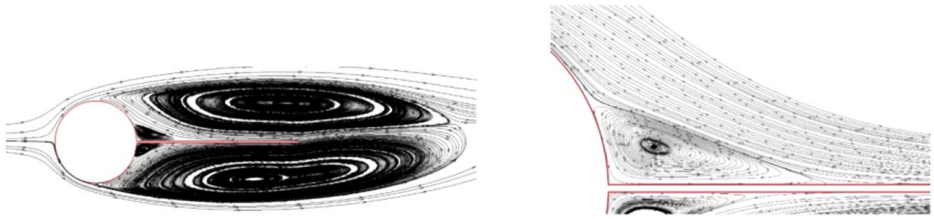

Fig. 10 Streamlines of the recirculation zone in the downstream of the cylinder

shows the vorticity contours for the flow past cylinder attached with SETE of varying lengths downstream of the cylinder. At Re = 100,000, vortex shedding delays even when the length of the plate (*L*/*D*) is 0.1. The formation of Von Karman Vortex Street has been observed up to the length of plate (*L*/*D*) = 0.5. It further delays as the length of the SETE increases. When length of the plate (*L*/*D*) is 0.6, the vortex shedding ceases. The vortex shedding for cylinders attached with SETE plates of length (*L*/*D*) more than 0.6 are not observed. At *L*/*D* = 0.1, for Reynolds number 100,000 a decrease of 5.35% in coefficient of drag, decrease of 41.82% in coefficient of lift has been observed. The Strouhal number remains the same as that of the circular cylinder case. When the ratio (*L*/*D*) is increased to 0.6, the vortex shedding stops and two large counter vortices are generated which extend to downstream of cylinder. A decrease of 21.67% in coefficient of drag, decrease of 92.60% in coefficient of lift, and a decrease of 45.83% in Strouhal number have been observed. From Figure 8, it can be observed that for *L*/*D* = 0.6, the *cl* (RMS) and *cd* (avg) are minimum compared to all other cases. The Strouhal number is also considerably low for this case. Moreover, from Fig. 9, it can be clearly observed that vortex shedding has stopped for this case. So, *L*/*D* = 0.6 is the optimal plate length.

Reason for Drag Reduction Using SETE

At the rear surface, the pressure drag is one of the prime contributors of drag in circular cylinder. When the vortex shedding occurs, a suction zone is formed, creating low-pressure region in downstream of cylinder. A high-pressure drag is experienced because of the high-pressure difference between upstream and the downstream of the cylinder. On the contrary, two attached vortices are generated due to SETE, improving the pressure recovery, and decreasing pressure drag when compared to the case where there are alternating shedding vortices (Fig. 10).

Hence, it can be said that the main reason for drag reduction is due to the seizure of the unsteady wake behavior. Gerrard [40] argued that for the shear layer to be shed from the surface, it should have a critical value of vorticity. The effect of attachment of splitter plate as observed from this research is to increase the recirculation length of the attached vortex. Increased recirculation length effectively increases diffusion of vorticity and hence the vorticity never reaches the critical value at which the shear layer sheds Gupta and Saha [41]. Hence as the plate length is increased, the vortex shedding gradually decreases and eventually stops after a critical length.

Conclusion

Flow over an isolated cylinder with a splitter plate attached to the rear surface has been numerically investigated and the optimal length of the splitter plate SETE is defined for decreasing the vortex shedding in the downstream of the cylinder. ANSYS FLUENT 2019 R3 has been used for simulating the cylinder at three Reynolds numbers, 100, 5000, and 100,000. The numerical model has been validated against existing literature and the grid independence study has been done for eliminating the influence of the number of grids on the computational results. The SST k–ω turbulence model has been selected for simulating the cylinder at different Reynolds numbers.

- The results have shown that with the increase in the length of the plate, the point from where the vortex shedding starts goes further downstream the cylinder.
- The frequency of vortex shedding is higher at high Reynolds number for the selected flow regime. This is concluded from observing the Strouhal number.
- For the circular cylinder case, at Re = 100 the St is 0.16, at Re = 5000 the St is 0.21, and for Re = 100,000 the St is 0.24.
- For Re = 100, the optimal plate length (*L*/*D*) is 1.5, for Re = 5000, the optimal plate length (*L*/*D*) is 1.2, and for Re = 100,000 the optimal plate length (*L*/*D*) is 0.6. On comparing all the cases, it can be deduced that the optimal plate length decreases with an increase in Reynolds number.
- The effectiveness of SETE increases with increase in Reynolds number.

- The current research could be extended to aero-acoustics for terminating the vortex phenomenon which can significantly improve cylinder's noise signature and could be of use especially for defense applications. Future research can be aimed for optimizing the shape and thickness of the splitter plate to further improve the aerodynamic performance of the cylinder. SETE could be incorporated with other various shapes of cylinders and airfoils for particular applications. Detailed study of the fluid-structure interaction also holds the key to the future of noiseless and fuel-efficient transportation.

Conflict of Interest

There are no conflicts of interest. This article does not include research in which human participants were involved. Informed consent not applicable. This article does not include any research in which animal participants were involved.

Data Availability Statement

The authors attest that all data for this study are included in the paper.

References

[1] Cao, D., Song, L., Li, J., Yuan, J., and Zhou, Y., 2014, "Determining the Drag Coefficient of a Cylinder Perpendicular to Water Flow by Numerical Simulation and Field Measurement," Ocean Eng., **85**(6), pp. 93–99.

[2] Opinel, P. A., and Srinil, N., 2020, "Application of Wake Oscillators to Two-Dimensional Vortex-Induced Vibrations of Circular Cylinders in Oscillatory Flows," J. Fluids Struct., **96**(4), p. 103040.

[3] Petersen, T. U., Mandviwalla, X., Christensen, E. D., Tarp-Johansen, N. J., and Rüdinger, F., 2020, "Oscillatory Loads on Circular Cylinder With Secondary Structures," J. Fluids Struct., **94**(28), p. 102935.

[4] Liu, J., and Gao, F. P., 2022, "Triggering Mechanics for Transverse Vibrations of a Circular Cylinder in a Shear Flow: Wall-Proximity Effects," J. Fluids Struct., **108**(12), p. 103423.

[5] Kang, S., 2006, "Uniform-Shear Flow Over a Circular Cylinder at Low Reynolds Numbers," J. Fluids Struct., **22**(4), pp. 541–555.

[6] Harichandan, A. B., and Roy, A., 2010, "Numerical Investigation of Low Reynolds Number Flow Past Two and Three Circular Cylinders Using Unstructured Grid CFR Scheme," Int. J. Heat Fluid Flow, **31**(2), pp. 154–171.

[7] Yang, W., and Stremler, M. A., 2019, "Critical Spacing of Stationary Tandem Circular Cylinders at Re≈100," J. Fluids Struct., **89**(4), pp. 49–60.

[8] Chen, W., Ji, C., Xu, D., and Srinil, N., 2019, "Wake Patterns of Freely Vibrating Side-by-Side Circular Cylinders in Laminar Flows," J. Fluids Struct., **89**(24), pp. 82–95.

[9] Ding, H., Shu, C., Yeo, K. S., and Xu, D., 2007, "Numerical Simulation of Flows Around Two Circular Cylinders by Mesh-Free Least Square-Based Finite Difference Methods," Int. J. Numer. Meth. Fluids, **53**(2), pp. 305–332.

[10] Meneghini, J. R., Saltara, F., Siqueira, C. L. R., and Ferrari, J. A., Jr., 2001, "Numerical Simulation of Flow Interference Between Two Circular Cylinders in Tandem and Side-By-Side Arrangement," J. Fluids Struct., **15**(2), pp. 327–350.

[11] Liu, T., Montefort, J., Liou, W., Pantula, S., and Shams, Q., 2007, "Lift Enhancement by Static Extended Trailing Edge," J. Aircraft, **44**(6), pp. 1939–1947.

[12] Imron, C., Widodo, B., and Yuwono, T. Y., 2018, "Reduction of Cd in Circular Cylinder Using 2 Passive Control at Re=1000 and 5000," J. Phys.: Conf. Ser., **974**(1), p. 01200.

[13] Roshko, A., 1961, "Experiments on the Flow Past a Circular Cylinder at Very High Reynolds Number," J. Fluid Mech., **10**(3), pp. 345–356.

[14] Kwon, K., and Choi, H., 1996, "Control of Laminar Vortex Shedding Behind a Circular Cylinder Using Splitter Plates," Phys. Fluids, **8**(2), pp. 479–486.

[15] Djebedjian, B., Renaudeaux, J., and Giat, M., 1996, "Numerical Study of the Drag Coefficient of an Infinite Circular Cylinder at Low and Moderate Reynolds Numbers Using the FLUENT Code."

[16] Liou, W., Pantula, S., Liu, T., Montefort, J., and Ludens, D., 2007, "Flow Past a Cylinder With a Flapping Element Attached to Its End," Am. Inst. Aeronaut. Astronaut., **45**(6), p. 1309.

[17] Lee, S. J., Lee, S. I., and Park, C. W., 2004, "Reducing the Drag on a Circular Cylinder by Upstream Installation of a Small Control Rod," Fluid Dyn. Res., **34**(2), pp. 233–250.

[18] Lim, H. C., and Lee, S. J., 2004, "Flow Control of a Circular Cylinder With O-Rings," Fluid Dyn. Res., **35**(2), pp. 233–250.

[19] Park, H., Lee, D., Jeon, W., Hahn, S., Kim, J., Kim, J., Choi, J., and Choi, H., 2006, "Drag Reduction in Flow Over a Two-Dimensional Bluff Body With a Blunt Trailing Edge Using a New Passive Device," J. Fluid Mech., **563**(17), pp. 389–414.

[20] Misirlioglu, A., Unal, M. F., and Bearman, P. W., 1993, *Passive Control of Wake From a Circular Cylinder With a Splitter Plate. International Union of Theoretical and Applied Mechanics*, Springer, Berlin, Heidelberg.

[21] Ozono, S., 1999, "Flow Control of Vortex Shedding by a Short Splitter Plate Asymmetrically Arranged Downstream of a Cylinder," Phys. Fluids, **11**(10), pp. 2928–2934.

[22] Vu, H. C., Ahn, J., and Hwang, J. H., 2016, "Numerical Investigation of Flow Around Circular Cylinder With Splitter Plate," KSCE J. Civ. Eng., **20**(6), pp. 2559–2568.

[23] Barman, B., and Bhattacharyya, S., "Control of Vortex Shedding and Drag Reduction Through Dual Splitter Plates Attached to a Square Cylinder," J. Marine. Sci. Appl., **14**(2), pp. 138–145.

[24] Pang, L. J. A., Skote, M., and Lim, S.-Y., 2016, "Modelling High Re Flow Around a 2D Cylindrical Bluff Body Using the k-ω (SST) Turbulence Model," Prog. Comput. Fluid Dyn., **16**(1), p. 48.

[25] Amalia, E., Moelyadi, M., and Ihsan, M., 2018, "Effects of Turbulence Model and Numerical Time Steps on Von Karman Flow Behavior and Drag Accuracy of Circular Cylinder," J. Phys.: Conf. Ser., **1005**(1), p. 012012.

[26] Duan, F., and Wang, J., 2021, "Fluid–Structure–Sound Interaction in Noise Reduction of a Circular Cylinder With Flexible Splitter Plate," J. Fluid Mech., **920**(10), p. A6-1.

[27] Mebarek-Oudina, F., Laouira, H., Hussein, A. K., Omri, M., Abderrahmane, A., Kolsi, L., and Biswal, U., 2022, "Mixed Convection Inside a Duct With an Open Trapezoidal Cavity Equipped With Two Discrete Heat Sources and Moving Walls," Mathematics, **10**(6), p. 929.

[28] Djebali, R., Mebarek-Oudina, F., and Choudhari, R., 2021, "Similarity Solution Analysis of Dynamic and Thermal Boundary Layers: Further Formulation Along a Vertical Flat Plate," Phys. Scr., **96**(8), p. 085206.

[29] Asogwa, K. K., Mebarek-Oudina, F., and Animasaun, I. L., 2022, "Comparative Investigation of Water-Based Al_2O_3 Nanoparticles Through Water-Based CuO Nanoparticles Over an Exponentially Accelerated Radiative Riga Plate Surface Via Heat Transport," Arab J. Sci. Eng., **47**(7), pp. 8721–8738.

[30] EL-Zahar, E. R., Rashad, A. M., Saad, W., and Seddek, L. F., 2020, "Magneto-Hybrid Nanofluids Flow Via Mixed Convection Past a Radiative Circular Cylinder," Sci. Rep., **10**(1), pp. 10494.

[31] Menter, F. R., 1992, Improved Two-Equation K-Omega Turbulence Models for Aerodynamic Flows (No. A-92183).

[32] Braza, M., Chassaing, P., and Ha Minh, H., 1986, "Numerical Study and Physical Analysis of the Pressure and Velocity Fields in the Near Wake of a Circular Cylinder," J. Fluid Mech., **163**(4), pp. 79–130.

[33] Tritton, D. J., 1959, "Experiments on the Flow Past a Circular Cylinder at Low Reynolds Numbers," J. Fluid Mech., **6**(4), p. 547.

[34] Wiesenberger, V. C., 1921, "Neuere festellungen über die Gesetze des üssigkeits und Luftwiderstands," Physik. Z, **22**(1), p. 231.

[35] Ahlborn, B., Seto, M., and Noack, B., 2002, "On Drag, Strouhal Number and Vortex-Street Structure," Fluid Dyn. Res., **30**(6), pp. 379–399.

[36] Widodo, B., Yuwono, T., and Imron, C., 2017, "The Influence of Distance Between Passive Control and Circular Cylinder on Wake," J. Phys.: Conf. Ser., **890**(1), p. 012053.

[37] Aljure, D. E., Lehmkhul, O., Rodríguez, I., and Oliva, A., 2017, "Three Dimensionality in the Wake of the Flow Around a Circular Cylinder at Reynolds Number 5000," J. Comput. Fluids, **147**(9), pp. 102–118.

[38] Cox, J., Brentner, K., Rumsey, C., and Younis, B., 1997, "Computation of Vortex Shedding and Radiated Sound for a Circular Cylinder," American Society of Mechanical Engineers, Aerospace Division (Publication) AD, 53-1, pp. 447–454.

[39] Zan, S. J., and Matsuda, K., 2002, "Steady and Unsteady Loading on a Roughened Circular Cylinder at Reynolds Numbers Up to 900,000," J. Wind Eng. Ind. Aerodyn., **90**(4–5), pp. 567–581.

[40] Gerrard, J. H., 1966, "The Mechanics of the Formation Region of Vortices Behind Bluff Bodies," J. Fluid Mech., **25**(2), pp. 401–413.

[41] Gupta, A., and Saha, A. K., 2019, "Suppression of Vortex Shedding in Flow Around a Square Cylinder Using Control Cylinder," Eur. J. Mech.—B/Fluids, **76**(31), pp. 276–291.